Femtosecond Ultraviolet−Visible Fluorescence Study of the Excited-State Proton-Transfer Reaction of 7-Azaindole Dimer

Satoshi Takeuchi and Tahei Tahara*

Institute for Molecular Science (IMS), Myodaiji, Okazaki 444-8585, Japan

Received: June 8, 1998; In Final Form: July 27, 1998

The dynamics of the excited-state proton-transfer reaction of 7-azaindole dimer has been investigated in hexane with use of the femtosecond fluorescence up-conversion method. Time-resolved measurements were performed in a wide fluorescence wavelength region from near-ultraviolet to visible (320−620 nm). Three fluorescence components due to the dimer were observed in addition to the fluorescence from coexisting monomer. Time-resolved fluorescence anisotropy measurements were also carried out, and the result indicated that the first (τ = 0.2 ps) and the second (τ = 1.1 ps) fluorescence components due to the dimer arise from two different dimeric excited states having different transition moment directions. The decay of the second component agrees with the rise of the third component, which is attributable to the fluorescence from the tautomeric excited state (τ = 3.2 ns) formed by the proton-transfer reaction. The fluorescence spectra of these three excited states were reconstructed from time-resolved fluorescence traces taken at 27 wavelengths, and they show intensity maxima around 330, 350, and 490 nm, respectively. This sequential red shift reflects the cascaded population relaxation after the photoexcitation. By combining the spectral data with fluorescence quantum yield data, the oscillator strengths of the three excited states were evaluated as 0.13, 0.048, and 0.023. We assigned the higher- and the lower-energy dimeric excited states to the "^1L_b" and "^1L_a" states of the dimer on the basis of the obtained photochemical information. The deuterium substitution effects were also examined for two isotopic analogues. It was concluded that the proton transfer proceeds exclusively from the lowest "^1L_a" excited state with a time constant of 1.1 ps, after the electronic relaxation takes place from the initially populated "^1L_b" state to the "^1L_a" state. The excited-state reaction pathway as well as quantitative characterization of each excited state is discussed.

1. Introduction

Proton transfer has been attracting considerable attention as one of the most fundamental reactions because of its crucial roles in a number of chemical and biochemical processes. From the viewpoint of photochemistry, the excited-state proton transfer is of particular interest, in which the reaction starts with photoexcitation. 7-Azaindole (Figure 1a) is a prototypical molecule showing this type of proton-transfer reaction. The dimer form of this molecule (Figure 2a) is structurally similar to hydrogen-bonded base pairs in DNA and has been regarded as a model system for the study of photoinduced mutation of the DNA base pairs.[1] It has been also shown that a tryptophan analogue incorporating the 7-azaindole chromophore (7-aza-tryptophan) functions effectively as a noninvasive fluorescent probe for the structure and dynamics of proteins.[2−4] Owing to this biochemical importance of 7-azaindole, the photochemistry and photophysics of this molecule have been central subjects of intense investigation for almost 3 decades, and its spectroscopic properties have been examined in a variety of environments.[5] Spectroscopic studies have revealed that 7-azaindole undergoes the photoinduced proton-transfer reaction in both protic and nonpolar solvents.

In alcohol solutions, it has been proposed that 7-azaindole forms a hydrogen-bonded 1:1 complex with a solvent molecule[1] (Figure 2b) and that the proton-transfer reaction proceeds in a two-step manner.[6] The first step involves reorganization of the solvent molecule around the photoexcited 7-azaindole to realize the conformation favorable for the proton transfer, and the second step is actual translocation of the two protons. In methanol solution, the complex before the reaction (and also nonreactive complex) gives fluorescence around 380 nm ("normal" fluorescence), while the tautomer species formed by the reaction emits fluorescence around 500 nm (tautomeric fluorescence). Time-resolved measurements on the normal and tautomeric fluorescences revealed that the proton-transfer time of the 7-azaindole−alcohol complex ranges from 100 to 300 ps at room temperature, depending on the alcohols.[6−9] In contrast to the 7-azaindole−alcohol complex, 7-azaindole in water shows only a single fluorescence band around 390 nm.[10] This significant difference in fluorescence spectra between the water complex and the alcohol complex has been discussed in detail, but the arguments seem still controversial, especially about the assignment of the single fluorescence band observed for the water complex and the quantum yield of the reaction.[11−15]

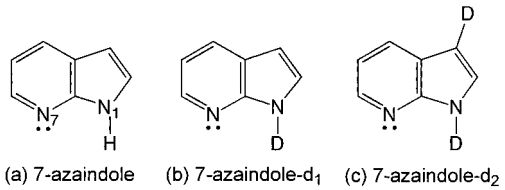

(a) 7-azaindole (b) 7-azaindole-d_1 (c) 7-azaindole-d_2

Figure 1. Molecular structures of 7-azaindole (a), N_1-deuterated 7-azaindole (b), and N_1- and C_3-deuterated 7-azaindole (c).

Although the reaction in protic solvents is solvent-mediated, the proton transfer in hydrocarbons takes place between two 7-azaindole molecules that form a cyclically hydrogen-bonded

* To whom correspondence should be addressed. Telephone: +81-564-55-7391. Fax: +81-564-54-2254.

S1089-5639(98)02522-5 CCC: $15.00
Published on Web 09/12/1998

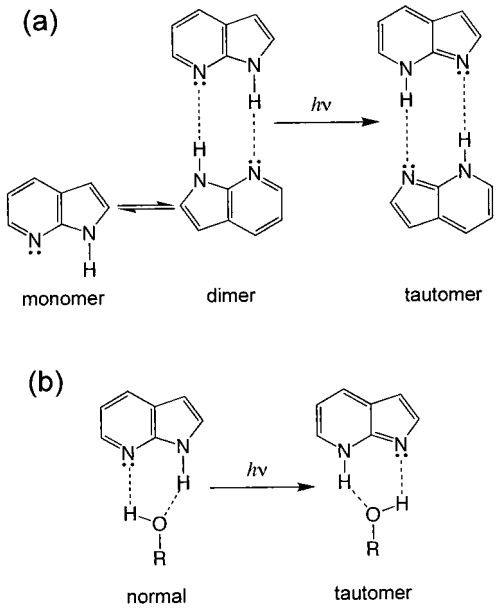

Figure 2. Photoinduced proton-transfer reaction of 7-azaindole. (a) Excited-state double-proton-transfer reaction of hydrogen-bonded 7-azaindole dimer in a hydrocarbon solution. Each proton is translocated from the pyrrolic nitrogen site (N_1) to the pyridinic nitrogen site (N_7). The dimer form is converted to the tautomer form by this reaction. The 7-azaindole monomer and dimer are in equilibrium in the ground state, and only the dimer undergoes this reaction. (b) Excited-state double-proton-transfer reaction of 7-azaindole in an alcohol solution. 7-Azaindole forms a cyclically hydrogen-bonded complex with a solvent molecule ("normal" species) in the ground state. The normal species undergoes the reaction, being converted to the tautomer species.

dimer[1] (Figure 2a). In this sense, the reaction dynamics in hydrocarbons is more directly related to the excited-state nature of 7-azaindole itself. In the singlet manifold of 7-azaindole, there are two closely lying electronic excited states that are analogous to the ^1L_a and ^1L_b states of polyacene systems.[16] It is expected that these "^1L_a" and "^1L_b" excited states take part in the excited-state relaxation and the proton-transfer reaction of 7-azaindole. Thus, the detailed knowledge about the nature of these excited states and their roles in the reaction are very important for a full understanding of the excited-state proton transfer of 7-azaindole. The 7-azaindole dimer provides a suitable system for the study of this problem.

The feasibility of the excited-state proton transfer of the 7-azaindole dimer is demonstrated in its fluorescence spectrum showing dual bands in the ultraviolet−visible region (Figure 3). It has been proposed[1] and confirmed later[17] that the longer-wavelength band ($\lambda_{max} = 490$ nm, "F_2" band) is due to the dimer and is assigned to the fluorescence from the tautomeric excited state formed by the proton-transfer reaction. The shorter wavelength band ($\lambda_{max} = 320$ nm, "F_1" band) showing a mirror image of the absorption spectrum is not due to the dimer but arises from the coexisting 7-azaindole monomer, which does not show any reactivity. The fluorescence from the dimeric excited state before the reaction cannot be recognized in the steady-state spectrum because of its very short lifetime. The intensity ratio of the F_1 to F_2 fluorescence bands has been extensively studied as a function of concentration, temperature, and excitation wavelength in order to obtain photochemical information on this reaction.[17−20]

Although the steady-state spectroscopic data can afford some information about the excited-state potential surface and the reaction mechanism, time-resolved measurements play a crucial role for elucidating the reaction dynamics and the excited-state

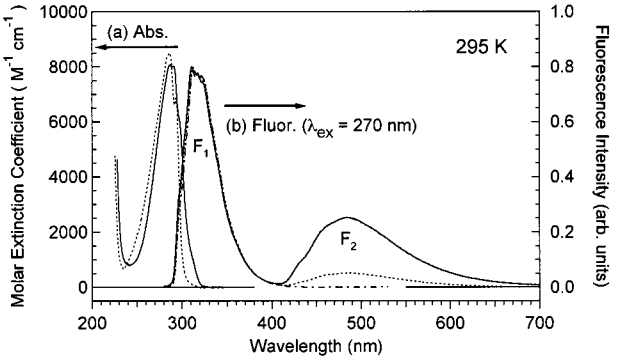

Figure 3. Steady-state absorption (left axis) and fluorescence (right axis) spectra of 7-azaindole in hexane at room temperature (295 K). (a) Absorption spectra of 7-azaindole monomer (- - -) and dimer (−). The monomeric spectrum was obtained from a dilute solution (1×10^{-5} mol dm^{-3}), while the dimeric spectrum was obtained by subtracting the monomeric contribution from absorption spectrum of a concentrated solution (1×10^{-3} mol dm^{-3}). The extinction coefficient of the dimer is normalized for one 7-azaindole molecule forming the dimer. (b) Steady-state fluorescence spectra obtained from 1×10^{-2} (−), 1×10^{-3} (- - -), and 1×10^{-5} (- · -) mol dm^{-3} solutions (270 nm excitation). These spectra were corrected for spectral sensitivity of the instrument and reabsorption of the sample.

properties of the 7-azaindole dimer. The first picosecond fluorescence study on the 7-azaindole dimer was reported in 1979, and it has revealed that the proton transfer occurs in less than 5 ps,[21] which is much faster than the proton transfer of the 7-azaindole−solvent complex in protic solvents. Femtosecond fluorescence study confirmed this rapid reaction of the dimer and reported that the reaction proceeds with a time constant as short as 1.4 ps at room temperature.[22] These time-resolved measurements, however, have been performed only on the tautomeric fluorescence, and the discussion was made on the basis of the time-resolved fluorescence data taken at a single wavelength. Thus, the spectroscopic data on the dimeric excited state before reaction are still very scarce. In a previous letter,[23] we reported our first femtosecond time-resolved fluorescence study of the 7-azaindole dimer. We performed up-conversion measurements for a wide fluorescence wavelength region from 420 to 620 nm and observed not only tautomeric fluorescence but also dimeric fluorescence. Furthermore, it was found that the dimeric fluorescence consists of two components that are assignable to the "^1L_a" and "^1L_b" states of the 7-azaindole dimer. We determined the proton-transfer time as 1.1 ps at room temperature by a fitting analysis, taking account of the contributions from these three excited states. We also discussed the effect of the excitation wavelength and solvent viscosity on the proton-transfer dynamics. In these measurements for the visible region, we observed spectral tails of the fluorescence bands due to the two dimeric excited states. Although almost all information on the proton-transfer dynamics is obtainable from these data, we were not able to get full information on the two dimeric excited states, including their fluorescence peak wavelengths and fluorescence transition probabilities. This lack of spectral information has left some ambiguity in the assignments of the dimeric excited states.

In this paper, we present a full account of our femtosecond fluorescence up-conversion study of the excited-state proton-transfer reaction of the 7-azaindole dimer in a nonpolar solvent. The fluorescence measurements were carried out in a wider wavelength region from near-ultraviolet to visible (320−620 nm), which revealed the whole spectral feature of the dimeric and tautomeric fluorescences. Time-resolved fluorescence anisotropy measurements were also performed. The evaluated

fluorescence transition energy, radiative lifetime, oscillator strength, and transition dipole moment direction give strong grounds for identification and characterization of the dimeric excited states that participate in the reaction. The isotope effect on the dynamics was also examined for two different deuterated analogues of 7-azaindole. On the basis of the obtained information, we discuss the reaction mechanism of the excited-state proton transfer of the 7-azaindole dimer.

2. Experimental Section

2.1. Time-Resolved Fluorescence Measurements. The experimental setup for the femtosecond up-conversion measurements is essentially the same as that described in detail previously.[24] Briefly, the light source is a mode-locked Ti:sapphire laser (Coherent, MIRA-900F) pumped by an argon ion laser (Coherent, INNOVA 310). The oscillator laser produces a 700 mW pulse train at a wavelength of 810 nm with a typical pulse duration of 55 fs. This fundamental pulse is converted to the third harmonic at 270 nm (30 mW) by using LiB_3O_5 (1 mm thickness) and β-BaB_2O_4 (1 mm thickness) crystals. The generated third harmonic is focused into a thin-film-like jet stream of the sample solution for the photoexcitation. The residual fundamental pulse after the third harmonic generation is used as a gate pulse for the up-conversion process. The fluorescence that is emitted from the sample is collected and focused into a β-BaB_2O_4 (0.5 mm thickness) mixing crystal with use of an aluminum-coated elliptic mirror. A cutoff filter (HOYA, L42, for visible fluorescence) or a band-pass filter (HOYA, B37, for near-ultraviolet fluorescence) is placed between the mirror and the mixing crystal to select the fluorescence component in the particular wavelength region of interest. The fluorescence is up-converted by type-I sum-frequency generation with the gate pulse in the mixing crystal. The up-converted signal is separated from the other lights by an iris, band-pass filters, and a 0.32 m monochromator (Jobin Yvon, HR-320) and is finally detected by a photomultiplier (Hamamatsu, R585) with a counter (Stanford Research Systems, SR400). The fluorescence detection at the magic angle is achieved by rotating the excitation polarization by a half-wave plate with respect to the gate polarization. The instrumental time resolution was estimated as 280 fs from the full width at half-maximum of a cross-correlation trace between the excitation and the gate pulses. The spectral resolution ranges from 10 to 14 nm, depending on the fluorescence wavelength.

Time-resolved fluorescence anisotropy data were also measured by using the same up-conversion spectrometer. In these anisotropy measurements, we masked the elliptic mirror and used only its central horizontal portion for the fluorescence collection in order to minimize contribution from different polarization components. The up-converted fluorescence intensities were measured with parallel ($I_{\parallel}$) and perpendicular ($I_{\perp}$) conditions at each delay time, and the following anisotropy value $r(t)$ was evaluated:

$$r(t) = \frac{I_{\parallel}(t) - I_{\perp}(t)}{I_{\parallel}(t) + 2I_{\perp}(t)} \qquad (1)$$

Time-resolved fluorescence data in the pico/nanosecond time region were collected by using the time-correlated single-photon-counting technique. The third harmonic (280 nm) of the same femtosecond oscillator laser is used as an excitation pulse, and it is loosely focused into a quartz cell (2 mm thickness) containing the sample solution. The residual fundamental pulse is used as a trigger pulse for the electronics. The emitted fluorescence is spectrally resolved (3 nm resolution) in a monochromator (Nikon, 250 mm focal length) and is detected by an MCP photomultiplier. The time resolution of the instrument is 150 ps as estimated from the full width at half-maximum of a trace monitoring the excitation pulse.

2.2. Steady-State Spectra and Fluorescence Quantum Yield. Steady-state absorption spectra were measured by a commercial spectrometer (Hitachi, U-3400).

Steady-state fluorescence spectra were measured with the photon-counting method in a 0° geometry by using a commercial spectrometer (Spex, Fluorolog-2). The correction was made for the spectral sensitivity of the instrument as well as for the reabsorption of the sample.

Fluorescence quantum yield of 7-azaindole in hexane was determined by comparing its fluorescence with that of quinine sulfate in 1 N sulfuric acid (1×10^{-4} mol dm^{-3}). The fluorescence quantum yield of this reference molecule has been accurately determined as $\eta_r = 0.55$.[25] We first measured the fluorescence spectrum of 7-azaindole in the *photon-number−density* representation as a function of *wavelength*, $S_q(\lambda)$ and then calculated the band intensities of the monomeric (F_M) and the tautomeric (F_T) fluorescences by integrating the spectrum over each wavelength region (290−410 nm for the monomer and 410−700 nm for the tautomer) as follows:

$$F_M \equiv \int_{290}^{410} S_q(\lambda)\, d\lambda \quad \text{and} \quad F_T \equiv \int_{410}^{700} S_q(\lambda)\, d\lambda \qquad (2)$$

Fluorescence band intensity of the reference (F_r) was also obtained by integrating its fluorescence spectrum over 350−700 nm. From these fluorescence band intensities, the fluorescence quantum yields of the monomeric (η_M) and the tautomeric (η_T) bands were evaluated by the following equation:[25]

$$\eta_i = \eta_r \frac{F_i}{F_r} \frac{1 - 10^{-OD_r}}{1 - 10^{-OD_s}} \frac{n_s^2}{n_r^2} \qquad (i = \text{M or T}) \qquad (3)$$

Here, OD_s and OD_r are optical densities of the 7-azaindole hexane solution and the reference solution, respectively, at the excitation wavelength, and $n_s = 1.3795$ (hexane) and $n_r = 1.3380$ (sulfuric acid aqueous solution) are refractive indices of the solvents.

2.3. Sample. 7-Azaindole was purchased from Aldrich Chemical Co. It was recrystallized twice from cyclohexane and subsequently dried in vacuo before use. N_1-Deuterated 7-azaindole (7-azaindole-d_1, Figure 1b) was obtained by refluxing a mixture of 7-azaindole (0.02 mol) and D_2O (5 mol) for 80 min under argon gas atmosphere. The 7-azaindole-d_1 was then recrystallized from the mixture and dried in vacuo. N_1 and C_3-deuterated 7-azaindole (7-azaindole-d_2, Figure 1c) was also obtained by similar refluxing but from an alkaline mixture of 7-azaindole (0.02 mol), D_2O (5 mol), and NaOD (0.07 mol). The position of the deuterium substitution and isotopic purity were checked by NMR and mass spectroscopies. The isotopic purities of the 7-azaindole-d_1 and 7-azaindole-d_2 were determined as $92 \pm 2\%$ and $>99\%$, respectively. Dehydrated hexane (water content less than 30 ppm) was received from Wako Pure Chemical Co., and it was further dried by molecular sieves. A fresh sample solution (1×10^{-2} mol dm^{-3}) was prepared for each scan of the time-resolved measurement.

3. Results and Discussion

3.1. Steady-State Properties of 7-Azaindole in Hexane. We first describe steady-state spectroscopic data of 7-azaindole in hexane. The steady-state properties described in this section are, in principle, already known. However, they are an indispensable basis for the discussion of time-resolved data.

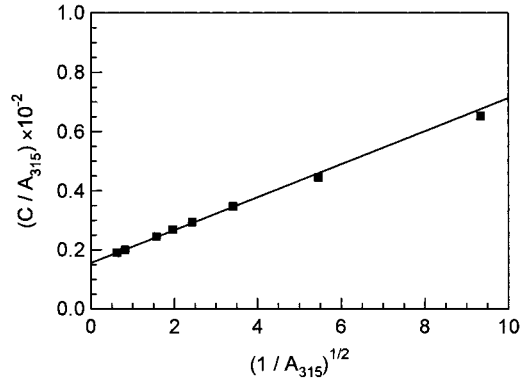

Figure 4. Plot of C/A_{315} against $(1/A_{315})^{1/2}$, where C is the concentration of the 7-azaindole hexane solution and A_{315} is its absorbance at 315 nm (1 cm path length). The solid squares are experimental data points measured for concentrations from 7.5×10^{-5} to 5×10^{-3} mol dm^{-3}. The straight line is the best fit to these data points. The slope and the intercept of this line give the equilibrium constant (K) for the dimerization of 7-azaindole (see text).

Several quantities obtained in this section are used in the analysis of femtosecond up-conversion data.

(a) Ground-State Monomer−Dimer Equilibrium and Their Absorption Spectra. 7-Azaindole in a dilute hexane solution exhibits the lowest-energy electronic absorption band in the region from 235 to 315 nm (Figure 3). This band is predominantly due to the 7-azaindole monomer. With increasing concentration, the absorption band extends to the longer wavelength region toward 325 nm. This change in the absorption band reflects self-association of 7-azaindole, i.e., formation of the dimer in which two intermolecular hydrogen bonds are formed between pyrrolic and pyridinic nitrogen sites[1] (Figure 2a). The concentration dependence of the absorption spectra indicates that the dimer has a slightly red-shifted absorption band compared with the monomer.[18,20]

The association constant (K) in hexane was evaluated from absorption spectra by a method described in the literature.[18] In this method, the equilibrium between the monomer (M) and the dimer (D), M + M $\leftrightarrow$ D, is assumed with a concentration relation of $[D] = K[M]^2$. The concentration of the dimer, [D], can be directly related to the absorbance at 315 nm (1 cm path length) as $A_{315} = 2\epsilon_D[D]$, since the monomer does not show any absorption at this wavelength. Here, ϵ_D is an extinction coefficient of the dimer at 315 nm. It should be noted that the ϵ_D value is normalized for one 7-azaindole molecule; a dimer is counted as two molecules. Then we obtain the following equation

$$\frac{C}{A_{315}} = \frac{1}{\epsilon_D} + \frac{1}{\sqrt{2\epsilon_D K}} \frac{1}{\sqrt{A_{315}}} \qquad (4)$$

where $C = [M] + 2[D]$ is the total concentration of the solution. This equation means that C/A_{315} is a linear function of $(1/A_{315})^{1/2}$. We measured the absorbance at 315 nm for several hexane solutions in the concentration range from 7.5×10^{-5} to 5×10^{-3} mol dm^{-3} at room temperature (295 K) and plotted C/A_{315} against $(1/A_{315})^{1/2}$ in Figure 4. From the slope and the intercept of the best-fitted line, we obtain $(1/(2\epsilon_D K))^{1/2} = 5.68 \times 10^{-4}$ and $1/\epsilon_D = 1.56 \times 10^{-3}$, which yield the association constant of $K = 2.4 \times 10^3$ M^{-1} and the dimer extinction coefficient of $\epsilon_D = 6.4 \times 10^2$ M^{-1} cm^{-1} at 315 nm. The obtained association constant for hexane solution is slightly larger than the value reported for the 3-methylpentane solution (1.8×10^3 M^{-1}),[18] but it is almost the same as that for the cyclohexane solution (2.2×10^3 M^{-1}).[26] Using the association constant, we can calculate a number ratio of the 7-azaindole molecules, which exist as the dimer in solution ("dimerization ratio"). The dimerization ratios of $\Delta(C) \equiv 2[D]/C = 0.044$, 0.444, 0.636, and 0.866 are obtained for hexane solutions of $C = 1 \times 10^{-5}$, 3×10^{-4}, 1×10^{-3}, and 1×10^{-2} mol dm^{-3}, respectively. This means that 86.6% of the 7-azaindole molecules form the dimer in a 1×10^{-2} mol dm^{-3} hexane solution.

Next we obtain the "pure" dimer spectrum with use of the association constant. The absorption spectrum of the monomer is obtainable simply from a dilute solution (e.g., 1×10^{-5} mol dm^{-3}) where the dimerization ratio is negligibly small. However, to obtain absorption spectrum of the dimer itself, we have to subtract the monomeric contribution from the absorption spectrum measured for a more concentrated solution. In a 1×10^{-3} mol dm^{-3} solution, for instance, 63.6% of 7-azaindole molecules exist as the dimer and 36.4% as the monomer. We subtracted the monomeric spectrum from the spectrum of this 1×10^{-3} mol dm^{-3} solution by taking account of the dimerization ratio. The obtained "pure" absorption spectrum of the dimer (solid curve) is compared with that of the monomer (dotted curve) in Figure 3. The absorption spectrum of the dimer is similar to that of the monomer but is red-shifted by ~10 nm. The oscillator strength is also obtained by integrating the absorption intensity over the lowest-energy band in each spectrum (integration over the 235−315 nm region for the monomer and over the 240−325 nm region for the dimer). The evaluated oscillator strength values, $f_M = 0.163$ (monomer) and $f_D = 0.159$ (dimer), are essentially the same as each other, implying that a similar electronic excited state(s) is responsible for the lowest-energy absorption bands of the monomer and the dimer.

(b) Steady-State Fluorescence Spectra. Steady-state fluorescence spectra of 7-azaindole in hexane excited at 270 nm are also shown in Figure 3 for three different concentrations. The fluorescence spectrum of the 1×10^{-5} mol dm^{-3} solution has a single band in the near-ultraviolet region from 290 to 410 nm (F_1 band). This F_1 band has been assigned to the 7-azaindole monomer. On the other hand, in the spectra of more concentrated solutions, another new fluorescence band appears in the visible region (F_2 band) in addition to the monomeric fluorescence band. This visible band is due to the dimer and has been assigned to the fluorescence from the tautomeric excited state.[1,17] It was reported that fluorescence excitation spectra monitoring the F_1 and the F_2 fluorescences coincide with the absorption spectra of the monomer and the dimer, respectively.[18,20] This fact implies that the interconversion between the monomer and the dimer is negligible in the excited state. Thus, the excited-state dynamics of the dimer can be considered separately from the monomer, although they coexist in solution.

When we discuss the fluorescence properties of 7-azaindole in hexane, we should note that the dimer−monomer ratio in the excited state is different from the ground-state equilibrium. It is because the excitation efficiencies of the monomer and the dimer are different from each other owing to the difference in the extinction coefficients at the excitation wavelength. Therefore, the dimer−monomer ratio in the excited state depends on both the dimerization ratio $\Delta(C)$ in the ground state and the extinction coefficient ratio $\Omega(\lambda_{ex}) \equiv \epsilon_D/\epsilon_M$ at the excitation wavelength. The initial concentration ratio of the excited dimer to all the excited molecules is expressed as

$$\kappa(\lambda_{ex}, C) \equiv \frac{2\epsilon_D[D]}{\epsilon_M[M] + 2\epsilon_D[D]} = \frac{\Omega(\lambda_{ex})\Delta(C)}{1 - \Delta(C) + \Omega(\lambda_{ex})\Delta(C)} \qquad (5)$$

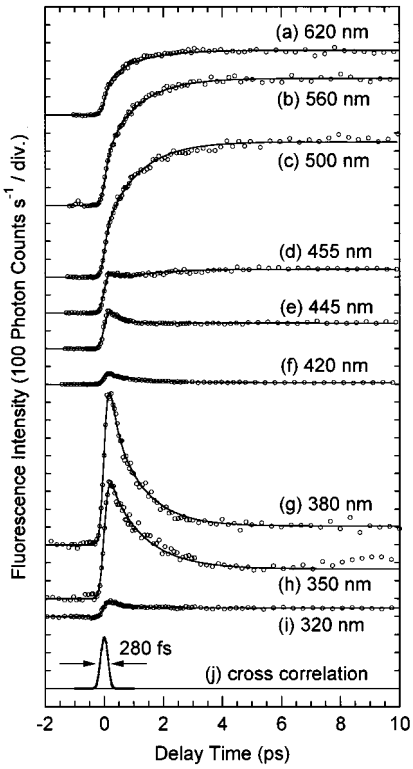

Figure 5. Up-converted fluorescence signals obtained from 7-azaindole in hexane (1×10^{-2} mol dm^{-3}, 270 nm excitation) at 620 nm (a), 560 nm (b), 500 nm (c), 455 nm (d), 445 nm (e), 420 nm (f), 380 nm (g), 350 nm (h), 320 nm (i), and a typical cross-correlation trace between the excitation and the gate pulses (j). The open circles are experimental data points, and the solid curves are results of the fitting analysis. The instrumental time resolution given by the fwhm of the cross-correlation trace is 280 fs.

From this equation, the κ value of 0.838 is calculated for the concentration of 1×10^{-2} mol dm^{-3} at the excitation wavelength of $\lambda_{ex} = 270$ nm. This means that 83.8% of the excited 7-azaindole molecules are present as the dimer while the rest (16.2%) are present as the monomer. The up-conversion measurements in the present study were performed under this condition.

3.2. Time-Resolved Fluorescence Data. Femtosecond time-resolved fluorescence was measured for a hexane solution (1×10^{-2} mol dm^{-3}) at 27 wavelengths in the region from near-ultraviolet to visible (320−620 nm) with use of the up-conversion method. Nine typical up-converted signals are shown in Figure 5. The excitation wavelength was 270 nm, and the excitation power was 20 mW. These data covering a wide wavelength region clearly show that the fluorescence temporal behavior varies drastically with change of the fluorescence wavelength. At long wavelengths (500−620 nm), a long-lived component with a finite rise time is observed. It is assignable to the fluorescence from the tautomeric excited state formed by the excited-state proton-transfer reaction ("tautomeric component"), because this wavelength region corresponds to the tautomeric fluorescence band (F_2 band) in the steady-state spectrum (Figure 3). At short wavelengths in the visible (420−455 nm), the fluorescence does not show the rise but exhibits a rapid decay, although a small contribution from the long-lived tautomeric component is still present. This rapid decay becomes much more prominent in the near-ultraviolet region (320−380 nm), where the tautomeric fluorescence is not observed. The long-lived component seen in this region is not the tautomeric component but is due to the 7-azaindole monomer ("monomeric component"). The observed wavelength-dependent fluorescence behavior shows that the fluorescence component(s) other than the long-lived monomeric and tautomeric components contributes to the observed signals, especially in the early delay time region.

In our previous paper[23] reporting time-resolved data in the visible region, we were able to extract the rapid decay observed in the short-wavelength region by eliminating the contribution of the copresent tautomeric component. It was found by the fitting analysis that the rapid decay is not a single exponential and that a biexponential function is required to obtain satisfactory results. The lifetimes of these two components were determined as $\tau_1 = 0.2 \pm 0.1$ ps ("ultrafast" component) and $\tau_2 = 1.1 \pm 0.1$ ps ("fast" component). The fluorescence data covering a wider wavelength region shown in Figure 5 confirm this conclusion. The double-exponential nature of the rapidly decaying fluorescence is now more clearly manifested in the near-ultraviolet region where the intensity peaks of these fluorescence components are located. The fluorescence temporal behavior in the entire observed region is explained with four fluorescence components in total: the ultrafast, fast, and tautomeric components due to the dimer and the coexisting monomeric fluorescence.

Of these four components, the ultrafast, fast, and tautomeric components are related to the proton-transfer reaction of the dimer. To clarify the reaction dynamics, we first discuss the rise time of the tautomeric component (τ_r), which directly represents the proton-transfer dynamics. Concerning the rise time of the tautomeric component, it is difficult to evaluate the time constant directly from the time-resolved signals at long wavelengths (500−620 nm) because the ultrafast and the fast components also contribute to the signal. However, as mentioned in the previous paper,[23] we obtained very clear information about the rise time of the tautomeric component from the time-resolved signal at 445 nm (Figure 5e). At this wavelength, the time-resolved fluorescence intensity becomes almost flat at delay times later than 1 ps when the ultrafast component vanishes completely and only the fast and tautomeric components contribute to the signal. This flatness indicates that the rise of the tautomeric component is completely canceled by the decay of the fast component. Thus, it is concluded that the rise time of the tautomeric component is equal to the decay time of the fast component, i.e., $\tau_r = \tau_2 = 1.1$ ps, and that the magnitudes of these two components are equal to each other at this particular wavelength (445 nm). At a slightly longer wavelength (455 nm) where the tautomeric component contributes more than the fast component, a rising feature is observed in the time region from 1 to 5 ps. On the other hand, a decaying feature is observed because of the larger contribution of the fast component at a shorter wavelength (420 nm). The agreement of the rise and the decay time constants strongly indicates that the fast component is due to the fluorescence from a dimeric excited state (P_2*) that undergoes the proton-transfer reaction.

As for the ultrafast component, it should be noted that a decaying feature is still observed in the time region from 0 to 1 ps even at 445 nm. This is unambiguous evidence for the existence of the ultrafast component. To clarify the origin of the ultrafast component, we measured time-resolved fluorescence anisotropy. The obtained anisotropy data at 500 and 380 nm are shown in Figure 6. At both wavelengths, we observed a very rapid decrease of the anisotropy immediately after photoexcitation (∼0.2 ps) in addition to a slow component attributable to the orientational diffusion of the 7-azaindole dimer. (Note that all three fluorescence components due to the dimer contribute to the signal at 500 nm.) This rapid fluorescence depolarization is indeed observed in the very early time

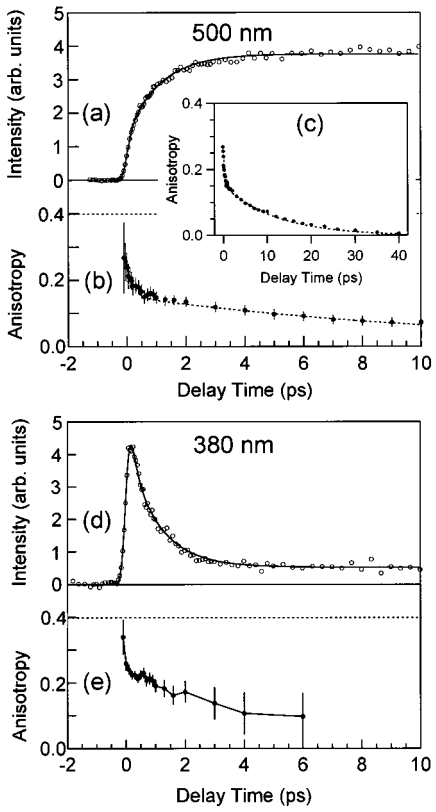

Figure 6. Time-resolved fluorescence anisotropy of 7-azaindole dimer in hexane. Upper panel shows the fluorescence signal (a) and the fluorescence anisotropy (b) measured at 500 nm. The longer-time behavior of the anisotropy is also shown in the inset (c). The dotted curve in the anisotropy data is the best-fitted biexponential function with decay time constants of 0.2 and 12 ps. Lower panel shows the fluorescence signal (d) and fluorescence anisotropy (e) measured at 380 nm. Note that the anisotropy data in this near-ultraviolet region contain contribution from the 7-azaindole monomer.

region shorter than 1 ps when the orientational motion of the dimer can be neglected. Thus, the rapid fluorescence depolarization is not due to the orientational motion but is ascribable to the change of transition moment direction of the excited-state itself, i.e., the change of the fluorescing state.[27] It is therefore highly likely that the rapid anisotropy change is caused by the internal conversion process from the initially populated excited state (P_1*) to the lower-lying second excited state (P_2*) having a different transition moment direction. The relaxation within a single electronic excited state does not cause such a drastic change of the anisotropy. Since the lifetime of the ultrafast component agrees with the time constant of the rapid anisotropy change, we concluded that the ultrafast component is due to the initially populated excited state (P_1*). The time constant of the orientational diffusion of the 7-azaindole dimer was also evaluated from the slow component seen in the anisotropy change. The obtained value (12 ps) is close to the reported orientational diffusion time of perylene (in hydrocarbon solvent),[28] which has similar shape and volume to those of the 7-azaindole dimer.

The femtosecond time-resolved fluorescence data shown in Figure 5 revealed that the electronic relaxation takes place from the first (P_1*) to the second (P_2*) excited states and that the proton transfer subsequently occurs from the second excited state. This scheme is further supported by experiments for deuterated analogues. In Figure 7, we compare time-resolved fluorescence signals obtained from normal 7-azaindole and its singly (7-azaindole-d_1) and doubly (7-azaindole-d_2) deuterated

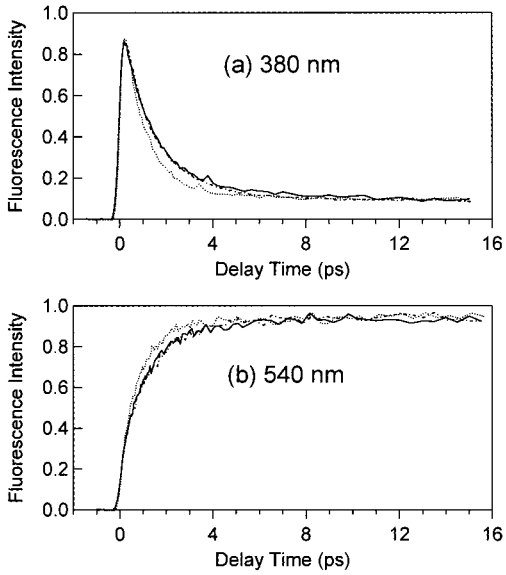

Figure 7. Deuterium substitution effect on the time-resolved fluorescence signals at 380 nm (a) and 540 nm (b). Fluorescence signals obtained from normal 7-azaindole (···), 7-azaindole-d_1 (−), and 7-azaindole-d_2 (- · -).

analogues. At both wavelengths, 380 and 540 nm, the three fluorescence signals behave very similarly to one another in the delay time range before 0.5 ps when the ultrafast component is dominant, while in the later time region the two isotopic analogues exhibit a slower time dependence than the normal 7-azaindole; the time constant of the fast component (τ_2) is affected by the deuterium substitution, but that of the ultrafast component (τ_1) is not. The difference in the deuterium substitution effects on the two time constants implies that only the fast component is relevant to actual translocation of the protons. Thus, we conclude that the proton-transfer reaction proceeds exclusively from the second excited state (P_2*). The time constant for the proton-transfer reaction changes from $\tau_2 = 1.1$ ps to $\tau_2 = 1.6$ ps by the deuteration at the N_1 site, but it is not affected by the deuteration at C_3 site.[29] This fact is a manifestation that the reaction coordinate is rather isolated in the NH···N part of the dimer.

The lifetimes of the monomeric and tautomeric fluorescences are too long to be determined in the up-conversion experiments. Although these long-lived species are not major subjects of the present work, the precise values of their lifetimes are required in the quantitative analysis, which is described in the next section. We determined these two lifetimes by using the time-correlated single-photon-counting method.

The monomeric fluorescence decays were measured at 325 nm for six hexane solutions having different concentrations. Some of the obtained data are shown in Figure 8. As clearly seen in this figure, the obtained decays are single exponentials for all the concentrations. However, we found that the lifetime significantly depends on the concentration. The monomeric fluorescence lifetimes (τ_4) evaluated by a fitting analysis are listed in Table 1. The lifetime in a low-concentration solution (1.6 ns) agrees well with a value reported for a dilute cyclohexane solution (1.67 ns[30]), but it becomes shorter with increasing concentration. The monomeric fluorescence lifetime is as short as $\tau_4 = 1.02$ ns in a 1×10^{-2} mol dm^{-3} solution, for which the present up-conversion measurements were made.

The tautomeric fluorescence decays were measured at 480 nm. The tautomeric fluorescence also exhibits a single-exponential decay. The obtained tautomeric fluorescence

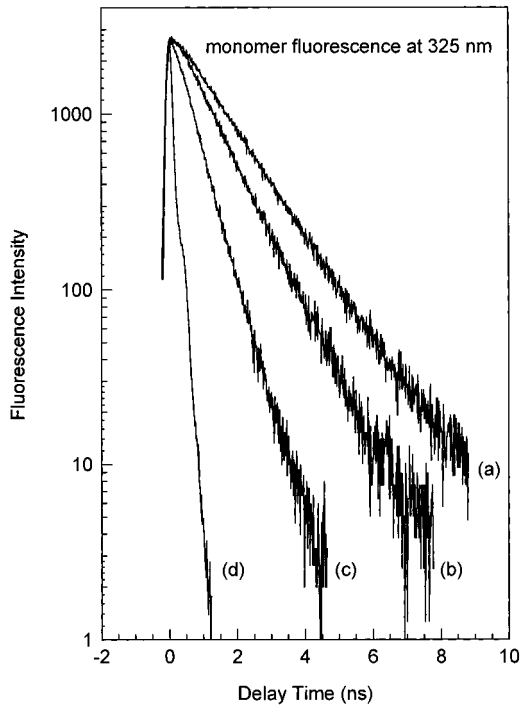

Figure 8. Concentration dependence of the monomeric fluorescence decays at 325 nm obtained from 7-azaindole in hexane at room temperature (280 nm excitation). Fluorescence decays are for concentrations of 1×10^{-5} (a), 1×10^{-2} (b), 3×10^{-2} mol dm^{-3} (c), and a typical instrumental response (d) is shown.

TABLE 1: Monomeric (τ_4) and Tautomeric (τ_3) Fluorescence Decay Times of 7-Azaindole and Its Deuterated Analogues

isomer	concentration (mol dm^{-3})	monomer τ_4 (ns)	tautomer τ_3 (ns)
7-azaindole	1×10^{-6}	1.60 ± 0.08	
	1×10^{-5}	1.51 ± 0.06	
	3×10^{-4}	1.24 ± 0.05	3.26 ± 0.10
	1×10^{-2}	1.02 ± 0.05	3.22 ± 0.10
	3×10^{-2}	0.55 ± 0.10	2.91 ± 0.10
	6×10^{-2}	0.38 ± 0.10	2.68 ± 0.10
7-azaindole-d_1	1×10^{-2}	1.01 ± 0.05	3.64 ± 0.10
7-azaindole-d_2	1×10^{-2}	1.05 ± 0.05	3.68 ± 0.10

lifetimes (τ_3) are listed in Table 1. In contrast to the monomeric fluorescence, the concentration dependence of the tautomeric fluorescence lifetime is recognized only in the high-concentration regime ($C > 1 \times 10^{-2}$ mol dm^{-3}). The lifetime is 3.22 ns for a 1×10^{-2} mol dm^{-3} solution, and essentially the same lifetime is obtained for more dilute solutions. This value is in good agreement with the literature values.[20,30]

We also measured the monomeric and tautomeric fluorescence lifetimes of the two deuterated analogues. The tautomeric fluorescence lifetime becomes 15% longer by the deuteration at the N_1 site, whereas the monomeric fluorescence lifetime does not change by deuteration at either the N_1 or C_1 site.

3.3. Fluorescence Spectra and Relative Oscillator Strengths. On the basis of the results obtained in the previous section, the excited-state dynamics of the 7-azaindole dimer is schematically depicted as follows:

$$\mathrm{D} \xrightarrow{h\nu} \mathrm{P_1}^* \xrightarrow{\tau_1} \mathrm{P_2}^* \xrightarrow{\tau_2} \mathrm{T}^* \xrightarrow{\tau_3} \mathrm{T} \tag{6}$$

where the labels D and T denote the dimer and tautomer, respectively, and the asterisk means the electronic excited states. The P_1* and P_2* stand for the two different dimeric excited states that give the ultrafast and fast fluorescence components. The lifetimes of the three excited states, τ_1, τ_2, and τ_3, have been experimentally determined as 0.2 ps, 1.1 ps, and 3.2 ns, respectively. In addition to the dimer, the monomer (M) also exists in hexane solution and gives monomeric fluorescence:

$$\mathrm{M} \xrightarrow{h\nu} \mathrm{M}^* \xrightarrow{\tau_4} \mathrm{M} \tag{7}$$

The lifetime of the monomeric excited state (τ_4) is 1.0 ns in the 1×10^{-2} mol dm^{-3} solution. In this section, we perform quantitative analysis on the femtosecond fluorescence data based on these schemes in order to obtain spectral information on each fluorescence component.

In the visible region, the ultrafast, fast and tautomeric fluorescence components contribute to the signal. Since they correspond to the fluorescences from the P_1*, P_2*, and T* states, respectively, the visible fluorescence can be represented as follows:

$$R_{\mathrm{vis}}(\lambda;t) = a_1(\lambda)[\mathrm{P_1}^*(t)] + a_2(\lambda)[\mathrm{P_2}^*(t)] + a_3(\lambda)[\mathrm{T}^*(t)] \tag{8}$$

In the ultraviolet region, on the other hand, the ultrafast, fast, and monomeric fluorescence components contribute to the signal so that we can express the ultraviolet fluorescence as follows:

$$R_{\mathrm{uv}}(\lambda;t) = a_1(\lambda)[\mathrm{P_1}^*(t)] + a_2(\lambda)[\mathrm{P_2}^*(t)] + a_4(\lambda)[\mathrm{M}^*(t)] \tag{9}$$

In these formulas, [P_1*(t)], [P_2*(t)], [T*(t)], and [M*(t)] represent population of the four excited states at time t, and $a_1(\lambda)$, $a_2(\lambda)$, $a_3(\lambda)$, and $a_4(\lambda)$ denote their intrinsic fluorescence transition probabilities at wavelength λ.

At first, we assume that the photoexcitation initially produces only the P_1* and M* states; neither P_2* nor T* state is populated at the time origin. By solving a set of simple rate equations based on the schemes 6 and 7 under this initial condition ([P_2*(0)] = [T*(0)] = 0), we obtain the following formulas for the population change of each excited state:

$$[\mathrm{P_1}^*(t)] = \mathrm{e}^{-K_1 t} \tag{10a}$$

$$[\mathrm{P_2}^*(t)] = \rho_{12}(\mathrm{e}^{-K_2 t} - \mathrm{e}^{-K_1 t}) \tag{10b}$$

$$[\mathrm{T}^*(t)] = \rho_{12}\rho_{23}\{(\mathrm{e}^{-K_3 t} - \mathrm{e}^{-K_2 t}) - \chi(\mathrm{e}^{-K_3 t} - \mathrm{e}^{-K_1 t})\} \tag{10c}$$

$$[\mathrm{M}^*(t)] = \frac{1-\kappa}{\kappa}\mathrm{e}^{-K_4 t} \tag{10d}$$

Consequently, we obtain the following functional forms for the time-resolved fluorescence signals in the visible and ultraviolet regions by combining formulas 8−10:

$$R_{\mathrm{vis}}(\lambda;t) = A_1(\lambda)\mathrm{e}^{-K_1 t} + A_2(\lambda)\mathrm{e}^{-K_2 t} + A_3(\lambda)\mathrm{e}^{-K_3 t} \tag{11}$$

$$a_1 = A_1 + A_2 + A_3, \quad a_2 = \frac{1}{\rho_{12}}A_2 + \frac{1}{\rho_{12}(1-\chi)}A_3, \quad \text{and} \quad a_3 = \frac{1}{\rho_{12}\rho_{23}(1-\chi)}A_3 \tag{12}$$

$$R_{\mathrm{uv}}(\lambda;t) = A_1(\lambda)\mathrm{e}^{-K_1 t} + A_2(\lambda)\mathrm{e}^{-K_2 t} + A_4(\lambda)\mathrm{e}^{-K_4 t} \tag{13}$$

$$a_1 = A_1 + A_2, \quad a_2 = \frac{1}{\rho_{12}}A_2, \quad \text{and} \quad a_4 = \frac{\kappa}{1-\kappa}A_4 \tag{14}$$

In these equations, $K_i \equiv 1/\tau_i$ denotes population relaxation rate of the P_1* (i = 1), P_2* (i = 2), T* (i = 3), and M* (i = 4) states, and $\chi = (K_2 - K_3)/(K_1 - K_3) \approx 0.182$, $\rho_{12} = K_1/(K_1 -$

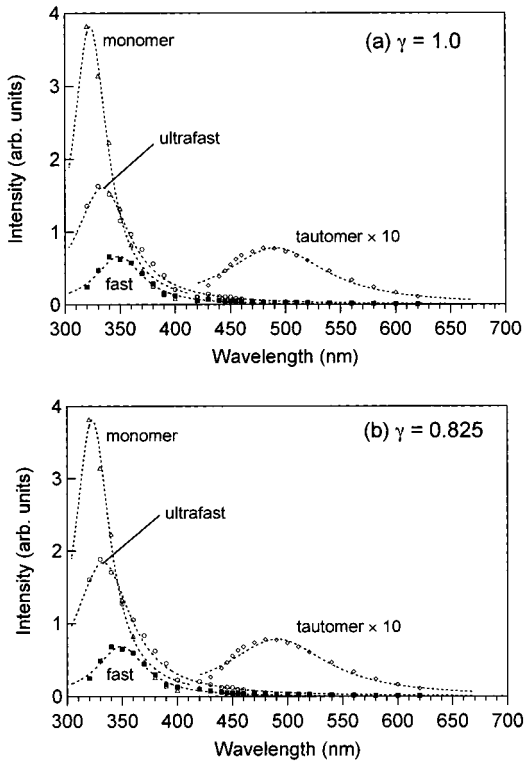

Figure 9. Fluorescence spectra of the four components obtained with $\gamma = 1.0$ (a) and $\gamma = 0.825$ (b) with the ultrafast (○), fast (■), tautomeric (◇), and monomeric (△) components in both plots. The dotted curves are the best-fitted Lorentzian functions. The tautomeric spectra are magnified 10 times.

$K_2) \approx 1.22$, and $\rho_{23} = K_2/(K_2 - K_3) \approx 1.00$. The factor of $(1 - \kappa)/\kappa = 0.162/0.838 \approx 0.193$ for the 1×10^{-2} mol dm^{-3} solution is included to take account of the initial concentration difference between the excited dimer and the excited monomer. We convoluted functions 11 and 13 with the instrumental response (Figure 5j) in order to take account of the finite time resolution and then fitted the resultant functions to the time-resolved fluorescence data by adjusting A_1, A_2, A_3, and A_4 values. The typical results of the fitting analysis are shown in Figure 5 (solid curves). The calculated curves successfully reproduced the observed fluorescence signals at all wavelengths, implying that the excited-state dynamics of 7-azaindole is well described by the schemes 6 and 7. From the obtained coefficients A_i, we calculated the a_i values by using relations 12 and 14.

The coefficients $a_1(\lambda)$, $a_2(\lambda)$, $a_3(\lambda)$, and $a_4(\lambda)$ represent fluorescence spectra of the four excited states P_1*, P_2*, T*, and M*, respectively. However, to reconstruct fluorescence spectra, we have to normalize these coefficients because the observed signal intensity is significantly influenced by the up-conversion efficiency, which depends on the fluorescence wavelength. Thus, we normalized the signal intensity (and hence the four coefficients) so that the time-integrated value of the signal is proportional to the steady-state fluorescence intensity (Figure 3) at each wavelength. The fluorescence spectra of the four components obtained after this intensity-normalization are shown in Figure 9a. As seen in this figure, the intensity maxima of the ultrafast and fast components are found in the near-ultraviolet region while that of the tautomeric component lies in the visible. These three spectra exhibit a sequential red shift, which is consistent with the cascaded relaxation process in scheme 6. The spectral shift between the first two components corresponds to the $P_1^* \rightarrow P_2^*$ electronic relaxation, while the large spectral change between the fast and the tautomeric components is associated with the proton-transfer reaction. In our previous paper,[23] we were able to report only spectral tails of the ultrafast and fast components. The present measurements covering a wider wavelength region from near-ultraviolet to visible allow us to observe entire spectral shapes of these components. It is also worth mentioning that the reconstructed spectrum of the monomeric component agrees well with the monomeric band (F_1 band) in the steady-state spectrum (Figure 3).

The normalized coefficient $a_i(\lambda)$ shown in Figure 9 also contains important information about the fluorescence transition probability of each excited state because the coefficient is proportional to the number of fluorescence photons emitted per unit time. The integration of the spectrum a_i in the frequency space

$$F_i \equiv \int_0^\infty a_i(\nu)\, \mathrm{d}\nu \tag{15}$$

yields a quantity that is proportional to the radiative decay rate of the excited state. By use of these F_i values, the ratio among the radiative decay rates (k_{ri}) of the P_1*, P_2*, T*, and M* states are expressed as $k_{r1}:k_{r2}:k_{r3}:k_{r4} = F_1:F_2:F_3:F_4$. To calculate the F_i values, we first converted the fluorescence spectrum in the wavelength space, $a_i(\lambda)$, to that in the frequency space, $a_i(\nu)$, using the relation $a_i(\nu) = \lambda^2 a_i(\lambda)$, and then replaced it by an adequate Lorentzian function:

$$a_i(\nu) \Rightarrow g_i(\nu) = G_i \frac{1}{\pi} \frac{\Gamma_i}{(\nu - \nu_{0i})^2 + \Gamma_i^2} \tag{16}$$

The best-fitted Lorentzian function reproduced each spectrum very well as shown in Figure 9 (dotted curves). By integration of the Lorentzian function, the F_i value is calculated as

$$F_i \cong \int_0^\infty g_i(\nu)\, \mathrm{d}\nu = G_i \tag{17}$$

From the G_i values, the ratio of the radiative decay rates is evaluated as $k_{r1}:k_{r2}:k_{r3}:k_{r4} = F_1:F_2:F_3:F_4 \cong G_1:G_2:G_3:G_4 = 0.667:0.244:0.0603:1.00$. The other parameters for the best-fitted Lorentzian functions, i.e., the central frequency (ν_{0i}) and the half bandwidth (Γ_i), are as follows: $\nu_{01} = 2.97 \times 10^4$ cm^{-1} and $\Gamma_1 = 2.67 \times 10^3$ cm^{-1} for the ultrafast component, $\nu_{02} = 2.85 \times 10^4$ cm^{-1} and $\Gamma_2 = 2.16 \times 10^3$ cm^{-1} for the fast component, $\nu_{03} = 2.01 \times 10^4$ cm^{-1} and $\Gamma_3 = 2.28 \times 10^3$ cm^{-1} for the tautomeric component, and $\nu_{04} = 3.09 \times 10^4$ cm^{-1} and $\Gamma_4 = 1.82 \times 10^3$ cm^{-1} for the monomeric component. Since the oscillator strength (f_i) is proportional to k_{ri}/ν_{0i}^2, the oscillator strength ratio among the P_1*, P_2*, T*, and M* states is also evaluated as $f_1:f_2:f_3:f_4 = k_{r1}/\nu_{01}^2:k_{r2}/\nu_{02}^2:k_{r3}/\nu_{03}^2:k_{r4}/\nu_{04}^2 = 0.722:0.287:0.143:1.00$.

The analysis described above has been made under the assumption that the dimer is directly photoexcited only to the P_1* state ("P_1* photoexcitation"). However, the obtained result indicates that the fluorescence spectra of the two dimeric excited states (P_1* and P_2*) are closely located, as shown in Figure 9a. This proximity in the fluorescence spectra suggests that their absorption spectra overlap each other and hence that the direct photoexcitation to the P_2* state ("P_2* photoexcitation") should also be considered. Thus, we next refine our analysis to take account of the P_2* photoexcitation as well.

To include the P_2* photoexcitation in the analysis, we solve the rate equations for the dimer under the initial condition of $[P_1^*(0)] = \gamma$, $[P_2^*(0)] = 1 - \gamma$, and $[T^*(0)] = 0$. This condition implies that both the P_1* and P_2* states are produced directly by the photoexcitation with a population ratio of γ: $(1-\gamma)$. Then

we obtain the following formulas representing the population change of the three excited states of the dimer:

$$[P_1^*(t)] = \gamma\, e^{-K_1 t} \tag{18a}$$

$$[P_2^*(t)] = \gamma\rho_{12}(e^{-K_2 t} - e^{-K_1 t}) + (1-\gamma)e^{-K_2 t} \tag{18b}$$

$$[T^*(t)] = \gamma\rho_{12}\rho_{23}\{(e^{-K_3 t} - e^{-K_2 t}) - \chi(e^{-K_3 t} - e^{-K_1 t})\} + (1-\gamma)\rho_{23}(e^{-K_3 t} - e^{-K_2 t}) \tag{18c}$$

In a practical sense, however, the change in this initial condition does not change the functional forms for the fitting analysis given in formulas 11 and 13 but only modifies the formulas connecting the parameters A_i with the coefficient $a_i(\lambda)$. Therefore, we do not have to repeat the fitting procedure from the beginning. Consequently, eqs 12 and 14 are revised as follows:

$$a_1 = \frac{1}{\gamma}A_1 + \frac{\rho_{12}}{\rho_{12}\gamma - \gamma + 1}A_2 + \frac{\rho_{12}(1-\chi)}{\rho_{12}\gamma - \gamma + 1 - \rho_{12}\gamma\chi}A_3$$

$$a_2 = \frac{1}{\rho_{12}\gamma - \gamma + 1}A_2 + \frac{1}{\rho_{12}\gamma - \gamma + 1 - \rho_{12}\gamma\chi}A_3 \tag{19}$$

$$a_3 = \frac{1}{\rho_{23}(\rho_{12}\gamma - \gamma + 1 - \rho_{12}\gamma\chi)}A_3$$

and

$$a_1 = \frac{1}{\gamma}A_1 + \frac{\rho_{12}}{\rho_{12}\gamma - \gamma + 1}A_2$$

$$a_2 = \frac{1}{\rho_{12}\gamma - \gamma + 1}A_2 \tag{20}$$

$$a_4 = \frac{\kappa}{1-\kappa}A_4$$

In the case of $\gamma = 1$, the eqs 19 and 20 become identical to the eqs 12 and 14, respectively. From the A_i values, which are determined uniquely by the experimental data, the time-resolved fluorescence spectra (a_i) and hence the oscillator strength ratio can be calculated for any value of γ.

The ratio between the P_1^* and the P_2^* photoexcitations is equal to the ratio of the extinction coefficients. Thus, the γ value, i.e., the ratio of the P_1^* photoexcitation to all the photoexcitations, can be represented as

$$\gamma = \frac{\epsilon_1}{\epsilon_1 + \epsilon_2} \tag{21}$$

where ϵ_1 and ϵ_2 are the extinction coefficients corresponding to the $P_1^* \leftarrow D$ and the $P_2^* \leftarrow D$ transitions at the excitation wavelength. Although this formula is very simple, we are not able to directly calculate this γ value because the absorption bands due to the $P_1^* \leftarrow D$ and $P_2^* \leftarrow D$ transitions have not been obtained separately. Therefore, we need to estimate this value on the basis of the fluorescence spectra, $a_1(\nu)$ and $a_2(\nu)$, and corresponding best-fitted Lorentzian functions, $g_1(\nu)$ and $g_2(\nu)$, which are obtained in the analysis. Here, we assume that (1) the mirror-image relationship holds between absorption and fluorescence and (2) the Stokes shifts between absorption and fluorescence are the same for both the $P_1^* \leftarrow D$ and the $P_2^* \leftarrow D$ transitions. Then, two functions, which are defined as $h_1(\nu) \equiv g_1(\nu)/{\nu_{01}}^2$ and $h_2(\nu) \equiv g_2(\nu)/{\nu_{02}}^2$, can be regarded as red-shifted "replicas" of the $P_1^* \leftarrow D$ and the $P_2^* \leftarrow D$ absorption bands, respectively. (Note that the Lorentzian function is symmetric so that the mirror-image projection just results in the red-shift in energy.) The factor $1/{\nu_{0i}}^2$ comes from the fact that the integration of the extinction coefficient over the absorption band is proportional not to the radiative decay rate but to the oscillator strength. Consequently, their sum, $h_1(\nu) + h_2(\nu)$, is considered as a "replica" of the observed dimer absorption. The three functions $h_1(\nu)$, $h_2(\nu)$, and $h_1(\nu) + h_2(\nu)$ are compared with the dimer absorption in Figure 10. From this figure, the peak frequencies of the "replica" and "real" absorption band are determined as $\nu_e = 2.93 \times 10^4$ cm^{-1} and $\nu_a = 3.47 \times 10^4$ cm^{-1} ($\lambda_{max} = 288$ nm), respectively, and their energy difference is $\delta = \nu_a - \nu_e = 5.4 \times 10^3$ cm^{-1}. Thus, the extinction coefficient ratio at the excitation wavelength ($\nu_{ex} = 3.70 \times 10^4$ cm^{-1}, 270 nm) is regarded as equivalent to the ratio of $h_1(\nu_p)$ to $h_2(\nu_p)$ values at the energy of $\nu_p = \nu_{ex} - \delta = 3.16 \times 10^4$ cm^{-1}. We obtained the γ value of 0.80 by this procedure. However, it should be noted that this value is calculated on the basis of the fluorescence spectra obtained by assuming $\gamma = 1.0$. In this sense, the obtained γ value needs further refinement.

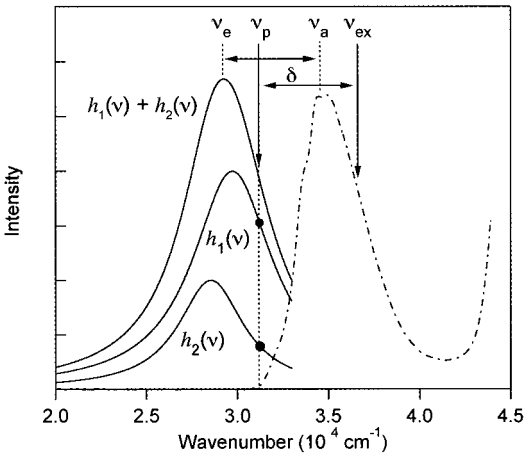

Figure 10. Red-shifted "replicas" of the $P_1^* \leftarrow D$ and $P_2^* \leftarrow D$ absorption bands, which are defined as $h_1(\nu) \equiv g_1(\nu)/{\nu_{01}}^2$ and $h_2(\nu) \equiv g_2(\nu)/{\nu_{02}}^2$, respectively, by using the best-fitted fluorescence spectra $g_i(\nu)$. The sum of these two can be regarded as a "replica" of the observed dimer absorption band (- · -). $\nu_{ex} = 3.70 \times 10^4$ cm^{-1} (270 nm) is the excitation frequency. $\nu_a = 3.47 \times 10^4$ cm^{-1} (288 nm) is the peak frequency of the dimeric absorption spectrum, and ν_e is the peak frequency of the red-shifted "replica" of the dimer absorption.

To determine the consistent "real" γ value, we repeated the above-described procedure iteratively. A γ value is estimated from the fluorescence spectra, and then fluorescence spectra are recalculated based on the new γ value by using eqs 19 and 20. In this iterative analysis, the γ value varied as $1.0 \rightarrow 0.80 \rightarrow 0.83 \rightarrow 0.8243 \rightarrow 0.8249$ and thus converged within the first several runs. Judging from this convergence of the γ value, we concluded that the "real" γ value is 0.825 and that 17.5% of the photoexcitation directly produces the P_2^* state. The fluorescence spectra calculated from this "real" γ value are shown in Figure 9b. This change of the γ value from 1.0 to 0.825 makes the relative amplitude of the P_1^* spectrum slightly larger with respect to the P_2^* spectrum. From these refined fluorescence spectra, we obtained the ratio of the F_i values as $F_1{:}F_2{:}F_3{:}F_4 = 0.779{:}0.255{:}0.0607{:}1.00$. The parameters for the final best-fitted Lorentzian functions are as follows: $\nu_{01} = 2.99 \times 10^4$ cm^{-1} ($\lambda_{max} = 332$ nm) and $\Gamma_1 = 2.74 \times 10^3$ cm^{-1} for the ultrafast component, $\nu_{02} = 2.85 \times 10^4$ cm^{-1} ($\lambda_{max} = 348$ nm) and $\Gamma_2 = 2.18 \times 10^3$ cm^{-1} for the fast component, $\nu_{03} = 2.01 \times 10^4$ cm^{-1} ($\lambda_{max} = 490$ nm) and $\Gamma_3 = 2.28 \times 10^3$ cm^{-1} for the tautomeric component, and $\nu_{04} = 3.09 \times 10^4$ cm^{-1} (λ_{max}

TABLE 2: Monomeric (ϕ_M) and Tautomeric (ϕ_T) Fluorescence Quantum Yields of 7-Azaindole Hexane Solutions Measured at Room Temperature (295 K)[a]

concentration (mol dm^{-3})	λ_{ex} (nm)	κ[b]	monomer			tautomer	
			η_M[c]	ϕ_M[d]	Φ^c_M[e]	η_T[c]	ϕ_T[d]
1×10^{-5}	270	0.035	0.190	0.197			
	280	0.040	0.195	0.203	0.201, 0.22,[f] 0.23,[g] 0.24[h]		
	290	0.051	0.211	0.222			
3×10^{-4}	270	0.389	0.0963	0.158		0.00762	0.0196
	280	0.419	0.0983	0.169	0.165	0.00869	0.0207
	290	0.484	0.0874	0.169		0.0107	0.0221
1×10^{-2}	270	0.838	0.0199	0.123		0.0164	0.0195
	280	0.854	0.0176	0.121	0.136, 0.1[i]	0.0169	0.0198, 0.02[i]
	290	0.884	0.0146	0.126		0.0188	0.0213

[a] 1×10^{-4} mol dm^{-3} quinine sulfate in 1 N sulfuric acid was used as a reference whose fluorescence quantum yield is 0.55. [b] Excited dimer ratio defined by formula 5. [c] Apparent fluorescence quantum yield. [d] Real fluorescence quantum yield evaluated by eqs 24 and 25. [e] Calculated fluorescence quantum yield. [f] Reference 13. [g] Reference 30. [h] Reference 10. [i] Reference 20.

$= 322$ nm) and $\Gamma_4 = 1.82 \times 10^3$ cm^{-1} for the monomeric component. The ratio of the oscillator strengths is also refined as $f_1:f_2:f_3:f_4 = 0.832:0.300:0.143:1.00$. The changes in the fluorescence spectra and relative oscillator strengths associated with the refinement are not large, but they cannot be neglected.

3.4. Absolute Oscillator Strengths and Related Quantities. Quantitative analysis of the up-conversion data afforded not only spectra but also relative oscillator strength values corresponding to the four fluorescence components. The oscillator strength is one of the most fundamental properties of the optical transition, and it manifests the nature of the excited state. Especially, the absolute oscillator strength values are important clues when we discuss the assignments of the two dimeric excited states P_1* and P_2*. Since the relative values are known, if we have one absolute value, we can evaluate all four oscillator strengths.

The oscillator strength is related to the radiative lifetime τ_{ri} (inverse of the radiative decay rate) of the excited state as follows:

$$f_i = \frac{mc/(8\pi^2 e^2)}{\nu_{0i}^2 \tau_{ri}} = \frac{1.499\text{cm}^{-2}\,\text{s}}{\nu_{0i}^2 \tau_{ri}} \qquad (22)$$

Since the fluorescence quantum yield (ϕ) is the ratio of the fluorescence lifetime (τ_i) to the radiative lifetime (τ_{ri}),

$$\phi = \frac{\tau_i}{\tau_{ri}} \qquad (23)$$

we can calculate the oscillator strength from the lifetime and quantum yield of the fluorescence. The lifetimes of the monomeric and tautomeric fluorescences have been determined as described in section 3.2. Thus, if we know their fluorescence quantum yields, we can calculate the absolute oscillator strengths by using eqs 22 and 23. In the case of 7-azaindole in nonpolar solvents, however, we should note that the real quantum yield ϕ is not obtainable directly from the measurements because the dimer and monomer coexist in the solution. The quantum yield that is obtained directly from the experiment is the apparent fluorescence quantum yield (η), which is defined as a ratio of the photon number emitted as fluorescence to the photon number absorbed by the *solution*. Thus, we have to calculate the real quantum yield from the apparent quantum yield by using the following equations:

$$\phi_T = \eta_T/\kappa \qquad \text{tautomeric fluorescence} \qquad (24)$$

$$\phi_M = \eta_M/(1-\kappa) \qquad \text{monomeric fluorescence} \qquad (25)$$

where κ is the excited dimer ratio defined by formula 5.

We measured the quantum yields of the monomeric and tautomeric fluorescences, and the results are summarized in Table 2. The measurements were made at room temperature (295 K) for hexane solutions having three different concentrations (1×10^{-5}, 3×10^{-4}, and 1×10^{-2} mol dm^{-3}) with use of three different excitation wavelengths ($\lambda_{ex} = 270$, 280, and 290 nm). As expected, the apparent quantum yields of the monomeric (η_M) and the tautomeric (η_T) fluorescences significantly depend on both concentration and excitation wavelength, reflecting the change in the monomer−dimer equilibrium and the extinction coefficient difference between the monomer and dimer at the excitation wavelength. The concentration dependence of the real quantum yield of the monomeric fluorescence (ϕ_M) is due to the concentration dependence of the monomeric fluorescence lifetime discussed in section 3.2 (see Table 1).

As for the monomeric fluorescence, we can also evaluate its quantum yield by using the radiative lifetime ($\tau_{Mr} = 7.52$ ns[31]), which is obtainable from the monomeric absorption spectrum. The quantum yield values calculated from the radiative and fluorescence lifetimes are $\Phi^c_M = \tau_4/\tau_{Mr} = 0.201$ (=1.51/7.52), 0.165 (=1.24/7.52), and 0.136 (=1.02/7.52) for the concentrations of 1×10^{-5}, 3×10^{-4}, and 1×10^{-2} mol dm^{-3}, respectively. The quantum yields obtained from the "direct" measurements (ϕ_M) agree very well with these calculated values (Φ^c_M). This agreement of the monomeric fluorescence quantum yields strongly indicates high reliability of our measurements. Thus, we can expect high reliability also for the tautomeric fluorescence quantum yield as well because the monomeric and tautomeric fluorescence quantum yields were measured simultaneously under completely identical conditions.

The quantum yield values of the tautomeric fluorescence (ϕ_T) are identical within experimental error, regardless of the difference in concentration or excitation wavelength. This is consistent with the fact that the tautomeric fluorescence lifetimes exhibit essentially no concentration dependence for the concentration range lower than 1×10^{-2} mol dm^{-3} (see Table 1). Thus, the quantum yield of the tautomeric fluorescence is safely determined as $\phi_T = 0.020 \pm 0.002$ for hexane solutions at room temperature from these sets of data. Since the quantum yield of the proton-transfer reaction is nearly unity, we can say that the fluorescence quantum yield of the tautomeric excited state (T*) is also 0.020 ± 0.002. The obtained quantum yield is in good agreement with the value reported for a 1×10^{-2} mol dm^{-3} 3-methylpentane solution.[20,32] Very recently, the quantum yield of the tautomeric fluorescence was measured by the time-resolved thermal lensing technique.[33] They reported the quantum yield value of 0.16, which is significantly larger than our value (0.02). Although the reason for this large discrepancy is

TABLE 3: Assignments and Properties of the Three Fluorescence Decay Components of the 7-Azaindole Dimer

	component		
	ultrafast	fast	long-lived
origin	dimeric ^1L_b	dimeric ^1L_a	tautomeric ^1L_a
peak wavelength (nm)	330	350	490
fluorescence lifetime (ps)	0.2	1.1	3220
radiative lifetime (ns)[a]	13	38	160
fluorescence quantum yield	1.5×10^{-5}	2.9×10^{-5}	2.0×10^{-2}
oscillator strength[b]	0.13	0.048	0.023

[a] Calculated for the transition frequencies at the fluorescence maximum. [b] Uncertainty is estimated as around 30%.

not clear at present, it seems that some error may be involved in their evaluation. In fact, the total fluorescence quantum yield of the methanol complex (0.08), which they obtained on the basis of their tautomeric fluorescence quantum yield, is also several times larger than other literature values (0.012 [8,13] $\approx$ 0.01 [30] in methanol; 0.013 [10] in ethanol).

With use of the quantum yield ($\phi_T = 0.02$) and the lifetime ($\tau_3 = 3.22$ ns in 1×10^{-2} mol dm^{-3} solution) of the tautomeric fluorescence in eq 23, we can now obtain the radiative lifetime of the tautomeric excited state (T*): $\tau_{r3} = \tau_3/\phi_T = 160$ ns. This value is very close to the radiative lifetime of the lowest excited singlet state of 7-methyl-7*H*-pyrrolo[2,3-*b*]pyridine (140 ns), which is a model molecule of the tautomer.[34,35] From this radiative lifetime and the fluorescence transition frequency ($\nu_{03} = 2.01 \times 10^4$ cm^{-1}), the absolute oscillator strength of the tautomeric excited state of the 7-azaindole dimer is evaluated as $f_3 = 0.023$ from eq 22. This value also shows good agreement with theoretical values obtained by semiempirical calculations (0.029,[36] 0.03,[34] and 0.031[20]). The oscillator strengths of the other three excited states are then evaluated as $f_1 = 0.13$, $f_2 = 0.048$, and $f_4 = 0.16$.[37] The obtained oscillator strength of the monomeric excited state (f_4) is consistent with the value estimated from the monomeric absorption spectrum ($f_M = 0.163$). The corresponding radiative lifetimes of the three excited states are $\tau_{r1} = 13$ ns, $\tau_{r2} = 38$ ns, and $\tau_{r4} = 9.8$ ns at their fluorescence transition frequencies (ν_{0i}).[38] Peak extinction coefficient for the transition from the ground state to each excited state can be estimated as $\epsilon_1 = 3.5 \times 10^3$ M^{-1} cm^{-1}, $\epsilon_2 = 1.6 \times 10^3$ M^{-1} cm^{-1}, $\epsilon_3 = 7.4 \times 10^2$ M^{-1} cm^{-1}, and $\epsilon_4 = 6.5 \times 10^3$ M^{-1} cm^{-1} if we assume the same band shapes for absorption and fluorescence and if we use the best-fitted Lorentzian given in eq 16. The fluorescence quantum yield of the three excited states are calculated from their radiative and fluorescence lifetimes: $\phi_1 = \tau_1/\tau_{r1} = 1.5 \times 10^{-5}$, $\phi_2 = 2.9 \times 10^{-5}$, and $\phi_4 = 0.11$.[38] These photochemical properties evaluated from the time-resolved fluorescence data and the fluorescence quantum yield data are summarized in Table 3 for the 7-azaindole dimer.

3.5. Assignments of the Two Precursor Excited States. To elucidate the mechanism and dynamics of the proton-transfer reaction of the 7-azaindole dimer, it is of great importance to identify the two dimeric excited states that are precursors of the reaction. Because of their very short lifetimes, fluorescences from the dimeric excited states are not recognized in steady-state spectra except for the case in which one lowers the temperature[18,21] or uses extreme red-edge excitation.[19,20,33] The detailed information on these excited states has been obtained for the first time in the present time-resolved study. In the following, we discuss assignments of the two dimeric excited states on the basis of their photochemical properties, which were evaluated in the previous sections.

In the singlet manifold of the 7-azaindole monomer, there exist two low-lying excited states that are analogous to the ^1L_a and ^1L_b states of linear condensed-ring molecules, polyacenes.[16] The ^1L_a and ^1L_b states of polyacenes are distinguished from each other by the difference in node distributions of their wave functions. Excitation energies of both states become lower with an increase of the number of the condensed rings, but the ^1L_a state is more effectively stabilized than the ^1L_b state. Thus, although the energy of the ^1L_a state is higher than the ^1L_b state in benzene, the state-ordering is reversed in tetracene. In naphthalene and anthracene, the two excited states are located closely in energy. Since 7-azaindole is an isoelectronic bicyclic analogue of naphthalene,[39] it is expected that the "^1L_a" and "^1L_b" states of this molecule are also located closely to each other. A semiempirical molecular-orbital calculation suggests that the lowest excited singlet state of 7-azaindole is the "^1L_b" state with an oscillator strength of 0.17 and that the "^1L_a" state having a smaller oscillator strength of 0.09 lies 2200 cm^{-1} above the "^1L_b" state.[40] In the solution phase, however, these two excited states are very likely located more closely because the "^1L_b" $\leftarrow$ S_0 and "^1L_a" $\leftarrow$ S_0 transitions cannot be resolved in the absorption spectrum. In fact, steady-state fluorescence excitation anisotropy data indicate that the "^1L_a" and "^1L_b" states of the 7-azaindole monomer are nearly degenerate and that their absorptions overlap completely to give the lowest-energy absorption band in solution[41] (Figure 3).

Upon dimerization, the absorption spectrum of the dimer shows a red shift of $\sim$ 10 nm with respect to that of the monomer, implying that the excited states of the monomer are somewhat affected by the dimerization. However, the oscillator strengths estimated from the lowest-energy bands of the monomeric and dimeric absorption spectra are $f_M = 0.163$ and $f_D = 0.159$, respectively, and they are essentially the same. This fact implies that the "^1L_a" and the "^1L_b" states also preserve their natures in the singlet manifold of the dimer and that they are responsible for the lowest-energy absorption band of the dimer. Since the sum of the oscillator strengths estimated for the two precursor excited states ($f_1 + f_2 = 0.13 + 0.048 = 0.18$) agrees well with the value obtained from the lowest-energy absorption band of the dimer ($f_D = 0.159$), we assigned the two precursor excited states to the "^1L_a" and "^1L_b" excited states of the dimer. In contrast to the case of the monomer, the fluorescence spectra of the two precursor excited states of the dimer are resolved with a peak-to-peak distance of 20 nm (=350 $-$ 330), as shown in Figure 9b. This indicates that the energy difference between the "^1L_a" and the "^1L_b" states of the dimer is larger than that of the monomer. In addition, our analysis showed that the first precursor excited state (P_1*) has a larger oscillator strength ($f_1 = 0.13$) than the second precursor excited state (P_2*; $f_2 = 0.048$). This means that in the 7-azaindole dimer the "^1L_b" state having a larger oscillator strength is located at a higher energy than the "^1L_a" state. This state-ordering is explainable in terms of the polar nature of the "^1L_a" state. It is known that a significant amount of the electron density flows from the pyrrolic to pyridinic moieties in the "^1L_a" state, yielding a dipole moment of 8.6 D that is considerably larger than those of the ground state (2.3 D) and the "^1L_b" state (3.4 D).[20] In the dimer, owing to the large dipole moment of the "^1L_a" state, it is highly likely that the dipole$-$dipole interaction between the two 7-azaindole molecules preferentially stabilizes the energy of this state and makes it substantially below the "^1L_b" state. Thus, we can conclude that the first (P_1*) and the second (P_2*) precursor excited states observed in the present time-resolved

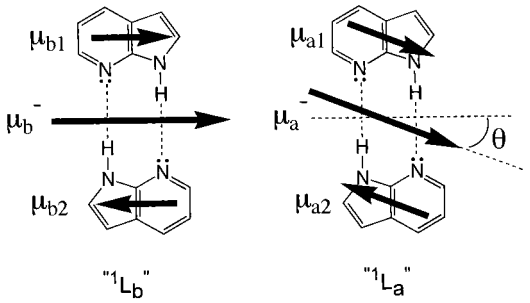

Figure 11. Transition dipole moments of the "^1L_b" and "^1L_a" excited states of the 7-azaindole dimer. The shorter arrow on each 7-azaindole molecule is a transition dipole moment of the monomer, while the longer arrow is that of the dimer. The transition moment of the "^1L_b" excited state is almost parallel with the molecular long axis, while that of the "^1L_a" excited state is tilted.

fluorescence measurements are the "^1L_b" and the "^1L_a" states of the dimer, respectively.

The nature of the "^1L_a" and "^1L_b" excited states in the dimer and their relevance to those of the monomer are worth mentioning. In the zeroth-order approximation, the ground (Ψ_0) and excited ($\Psi_a^{\pm}$ and $\Psi_b^{\pm}$) states of the dimer can be described by the following combinations of the monomeric wave functions:[1]

$$\Psi_0 = |g_1\rangle|g_2\rangle$$

$$\Psi_a^{\pm} = \{|a_1\rangle|g_2\rangle \pm |g_1\rangle|a_2\rangle\}/\sqrt{2} \qquad (26)$$

$$\Psi_b^{\pm} = \{|b_1\rangle|g_2\rangle \pm |g_1\rangle|b_2\rangle\}/\sqrt{2}$$

where $|a_i\rangle$ and $|b_i\rangle$ are the "^1L_a" and "^1L_b" excited states of the monomer, respectively, and the subscript $i = 1$ or 2 distinguishes each 7-azaindole molecule in the dimer. These expressions mean that each excited state of the monomer splits into two upon dimerization. Assuming a symmetric planar structure for the 7-azaindole dimer, these two splitted states have A_g symmetry (Ψ_a^+ and Ψ_b^+) and B_u symmetry (Ψ_a^- and Ψ_b^-), respectively. In our previous paper,[23] we mentioned these splitted A_g and B_u states as possible, but much less likely, candidates for the two precursor excited states, i.e., Ψ_a^+ and Ψ_a^- or Ψ_b^+ and Ψ_b^-. This possibility is now ruled out by a consideration of the transition probabilities from the ground state. The transition dipole moments of the splitted states are calculated using the wave functions given in eq 26, and they are expressed as the sum or difference of the monomeric transition moments:

$$\mu_a^{\pm} \equiv \langle \Psi_a^{\pm}|\mu|\Psi_0\rangle = (\mu_{a1} \pm \mu_{a2})/\sqrt{2}$$

$$\mu_b^{\pm} \equiv \langle \Psi_b^{\pm}|\mu|\Psi_0\rangle = (\mu_{b1} \pm \mu_{b2})/\sqrt{2} \qquad (27)$$

with

$$\mu_{ai} = \langle a_i|\mu|g_i\rangle \quad \text{and} \quad \mu_{bi} = \langle b_i|\mu|g_i\rangle$$

where μ is electronic dipole operator. These formulas show that in the A_g states (Ψ_a^+ and Ψ_b^+) the monomeric transition dipoles cancel each other and that the A_g states have no transition probabilities from the ground state. (Note that the transition moment vectors of the two monomers are antiparallel as shown in Figure 11.) This rigorous one-photon forbiddeness of the A_g states is in sharp contrast to the evaluated oscillator strengths of the two precursor excited states ($f_1 = 0.13$ and $f_2 = 0.048$). Thus, it is concluded that the first and the second precursor excited states of the dimer are both of B_u symmetry and are expressed as Ψ_b^- and Ψ_a^-, respectively.

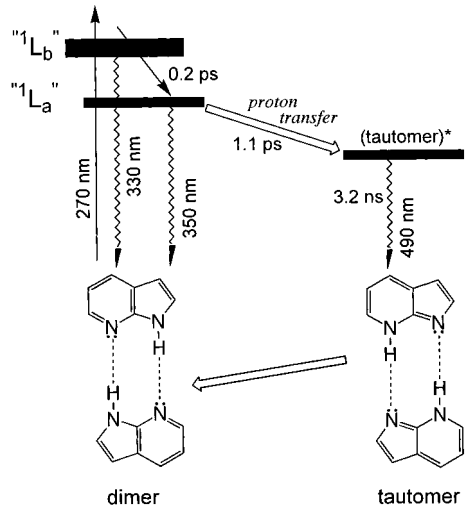

Figure 12. Schematic energy diagram illustrating the dynamics of the excited-state double-proton-transfer reaction of 7-azaindole dimer.

Formula 27 shows that the transition moment directions of the first (μ_b^-) and the second (μ_a^-) precursor excited states are parallel to those of the "^1L_b" and "^1L_a" states of the monomer, respectively. It was reported by a semiempirical molecular-orbital calculation that the transition moment direction of the "^1L_b" state of the 7-azaindole monomer is almost collinear with the molecular long axis, while that of the "^1L_a" state is tilted by 23°.[40] Because of the asymmetric structure of the 7-azaindole molecule, the dipole moments of the "^1L_a" and "^1L_b" states are not perpendicular to each other. Thus, also in the dimer, it is highly likely that the transition moment of the first precursor excited state ("^1L_b") is directed almost parallel to the molecular long axis, while that of the second precursor excited state ("^1L_a") is tilted. The rapid fluorescence anisotropy change observed immediately after photoexcitation in the present study is consistent with this difference in the transition moments of the two excited states. As shown in Figure 6, the fluorescence anisotropy obtained from the 7-azaindole dimer exhibits a rapid decay from 0.27 to ~0.15 in the first 0.5 ps, reflecting the electronic relaxation from the "^1L_b" to "^1L_a" excited states. The anisotropy value after this rapid decay (0.15) is significantly larger than −0.2, which is expected for the transition perpendicular to the excitation polarization.[27] This is, therefore, clear experimental evidence that the transition moment directions of the two precursor excited states of the 7-azaindole dimer are different but are far from perpendicular.[42] The deviation of the observed initial anisotropy value (0.27) from the ordinary 0.4 is probably due to the finite time resolution of our measurements.

3.6. Proton-Transfer Reaction Dynamics of 7-Azaindole Dimer. Figure 12 illustrates the dynamics of the excited-state proton-transfer reaction of 7-azaindole dimer in hexane, which has been clarified in the present study. This photochemical reaction involves two ground-state isomers (dimer and tautomer) and three excited states, i.e., two dimeric excited states and tautomeric excited state, forming a cyclic reaction pathway. The excited-state dynamics of this reaction can be summarized as follows.

The photoexcitation at 270 nm directly produces both the "^1L_b" and "^1L_a" excited states in the singlet manifold of the dimer because of considerable overlapping of their absorption bands. Our analysis shows that 82.5% of the excited dimers

are initially populated in the "^1L_b" state while the rest is in the "^1L_a" state under our experimental conditions. The "^1L_b" state emits fluorescence around 330 nm, which is red-shifted by ~10 nm from the monomeric fluorescence. The "^1L_b" state relaxes to the "^1L_a" state, which is the lowest excited singlet state of the dimer, with a time constant of 0.2 ps. The fluorescence from this "^1L_a" state is observed around 350 nm, which is 20 nm red-shifted from the "^1L_b" fluorescence. The large energy spacing between the "^1L_b" and "^1L_a" states in the dimer comes from preferential energy stabilization of the polar "^1L_a" state. After rapid internal conversion from the "^1L_b" state to the "^1L_a" state, the proton-transfer reaction takes place exclusively from the lowest "^1L_a" state with a time constant of 1.1 ps. This selective reaction pathway from the "^1L_a" state is attributable to the high acidity at the pyrrolic nitrogen site in this state.[20] In other words, the enhanced proton-donating ability of the "^1L_a" state is a driving force for the proton-transfer reaction. The higher reactivity of the "^1L_a" state over the "^1L_b" state can also be understood in terms of a nodal plane analysis of their wave functions.[43]

It is worth mentioning that a stepwise reaction mechanism was recently proposed for the proton transfer of the 7-azaindole dimer in a supersonic jet beam.[44−46] Douhal et al.[44] have performed femtosecond pump−probe mass spectroscopy for jet-cooled 7-azaindole dimer and found two decay components in the time-resolved ion signals. They assigned these two components to a dimeric excited state and a zwitterionic intermediate in which only one proton is translocated. Since the two time constants (0.2 and 1.6 ps) are similar to those obtained in the present study ($\tau_1 = 0.2$ ps and $\tau_2 = 1.1$ ps), one may think that the "fast" fluorescence component might be assignable to the zwitterionic state. However, this possibility is easily excluded by the following two arguments. First, since the zwitterionic state is a cation−anion pair by nature, its fluorescence spectrum is expected to resemble that of protonated 7-azaindole at the pyridinic nitrogen site (N_7). It was reported that the protonated 7-azaindole cation exhibits a single fluorescence band peaked at 450 nm in ethanol−HCl solution[1], at 430 nm in acidic aqueous solution (pH < 4),[11] and at 420 nm in a highly acidic alcohol solution (1,1,1,3,3,3-hexafluoropropan-2-ol).[30] Consequently, the zwitterionic state is expected to emit fluorescence in the 420−450 nm region. This fluorescence peak wavelength is totally different from that of the second precursor excited state, which has been revealed in the present study (350 nm). Second, if the ultrafast component involves the motion of the first proton to form the zwitterionic intermediate, it should be affected by the deuterium substitution. As clearly shown in Figure 7, however, the time constant of the ultrafast component ($\tau_1 = 0.2$ ps) remains unchanged by the deuterium substitution at the N_1 site, indicating that the ultrafast component is not relevant to the actual translocation of the proton. Therefore, at least in solution, it is highly probable that the proton-transfer reaction of 7-azaindole dimer proceeds not in a stepwise but in a concerted way.

The proton-transfer reaction converts the "^1L_a" excited state of the dimer to the tautomeric excited state in which both protons are translocated from pyrrolic to pyridinic nitrogen sites. This "product" excited state emits largely Stokes shifted green fluorescence around 490 nm. As shown for a model molecule of the tautomer, 7-methyl-7*H*-pyrrolo[2,3-*b*]pyridine, the lowest excited singlet state of the tautomer is also of "^1L_a" character.[20] The large Stokes shift observed for the tautomeric excited state is a manifestation of large stabilization energy gained by the highly polar ^1L_a character of this state. The proton-transfer reaction of the 7-azaindole dimer proceeds from the dimeric to the tautomeric excited states with conservation of the ^1L_a character of the electronic states. The tautomeric excited state subsequently relaxes to the tautomeric ground state with a time constant of 3.2 ns. The tautomer form is less stable than the dimeric form in the electronic ground state so that back proton transfer takes place and the reaction is completed by forming the original dimeric ground state.[47]

While preparing this paper, we found a letter[48] reporting femtosecond fluorescence dynamics of the 7-azaindole dimer in hexadecane. In the letter, they mentioned slow dynamics (12 ps) observed in the tautomeric fluorescence at 480 nm and claimed that it is an indication of the existence of the zwitterionic intermediate in the proton-transfer reaction. This slow dynamics has been also recognized in our measurements, although this component is less prominent in hexane we used (e.g., see up-conversion signal at 500 nm in Figure 5). We found, however, that this slow component appears as a rise around the intensity maximum of the tautomeric fluorescence but gives a decay at the red edge of the fluorescence band (560−600 nm). Judging from the reconstructed time-resolved spectra, we think that this slow component is not due to the population dynamics but arises from the small spectral change ("sharpening") of the tautomer band. Since the time constant (12 ps) is a typical value for the vibrational cooling process in hydrocarbons,[49] we assigned this dynamics to the vibrational relaxation in the tautomeric excited state and did not include it in our analysis. In fact, we have observed very similar fluorescence dynamics also for a polyacene, which does not show any reaction.[50] Finally, we stress that regardless of its assignment, our quantitative arguments on the dimeric and tautomeric excited states are not affected by the existence of this slow dynamics because the corresponding spectral change is small.

Acknowledgment. The authors thank Dr. M. Tomura at the Research Center for Molecular Materials, IMS, for his valuable comments on deuterium substitution of 7-azaindole.

References and Notes

(1) Taylor, C. A.; El-Bayoumi, M. A.; Kasha, M. *Proc. Natl. Acad. Sci. U.S.A.* **1969**, *63*, 253.
(2) Negrerie, M.; Bellefeuille, S. M.; Whitham, S.; Petrich, J. W.; Thornburg, R. W. *J. Am. Chem. Soc.* **1990**, *112*, 7419.
(3) Rich, R. L.; Negrerie, M.; Li, J.; Elliott, S.; Thornburg, R. W.; Petrich, J. W. *Photochem. Photobiol.* **1993**, *58*, 28.
(4) Chen, Y.; Gai, F.; Petrich, J. W. *J. Phys. Chem.* **1994**, *98*, 2203.
(5) Smirnov, A. V.; English, D. S.; Rich, R. L.; Lane, J.; Teyton, L.; Schwabacher, A. W.; Luo, S.; Thornburg, R. W.; Petrich, J. W. *J. Phys. Chem. B* **1997**, *101*, 2758.
(6) McMorrow, D.; Aartsma, T. J. *Chem. Phys. Lett.* **1986**, *125*, 581.
(7) Moog, R. S.; Bovino, S. C.; Simon, J. D. *J. Phys. Chem.* **1988**, *92*, 6545.
(8) Moog, R. S.; Maroncelli, M. *J. Phys. Chem.* **1991**, *95*, 10359.
(9) Chen, Y.; Gai, F.; Petrich, J. W. *J. Am. Chem. Soc.* **1993**, *115*, 10158.
(10) Avouris, P.; Yang, L. L.; El-Bayoumi, M. A. *Photochem. Photobiol.* **1976**, *24*, 211.
(11) Negrerie, M.; Gai, F.; Bellefeuille, S. M.; Petrich, J. W. *J. Phys. Chem.* **1991**, *95*, 8663.
(12) Chou, P.-T.; Martinez, M. L.; Cooper, W. C. *J. Phys. Chem.* **1992**, *96*, 5203.
(13) Chapman, C. F.; Maroncelli, M. *J. Phys. Chem.* **1992**, *96*, 8430.
(14) Gai, F.; Chen, Y.; Petrich, J. W. *J. Am. Chem. Soc.* **1992**, *114*, 8343.
(15) Chen, Y.; Rich, R. L.; Gai, F.; Petrich, J. W. *J. Phys. Chem.* **1993**, *97*, 1770.
(16) Platt, J. R. *J. Chem. Phys.* **1949**, *17*, 484.
(17) Ingham, K. C.; Abu-Elgheit, M.; El-Bayoumi, M. A. *J. Am. Chem. Soc.* **1971**, *93*, 5023.
(18) Ingham, K. C.; El-Bayoumi, M. A. *J. Am. Chem. Soc.* **1974**, *96*, 1674.

(19) Waluk, J.; Bulska, H.; Pakula, B.; Sepiol, J. *J. Lumin.* **1981**, *24/25*, 519.
(20) Bulska, H.; Grabowska, A.; Pakula, B.; Sepiol, J.; Waluk, J.; Wild, U. P. *J. Lumin.* **1984**, *29*, 65.
(21) Hetherington, W. M.; Micheels, R. H.; Eisenthal, K. B. *Chem. Phys. Lett.* **1979**, *66*, 230.
(22) Share, P.; Pereira, M.; Sarisky, M.; Repinec, S.; Hochstrasser, R. M. *J. Lumin* **1991**, *48/49*, 204.
(23) Takeuchi, S.; Tahara, T. *Chem. Phys. Lett.* **1997**, *277*, 340.
(24) Takeuchi, S.; Tahara, T. *J. Phys. Chem. A* **1997**, *101*, 3052.
(25) Demas, J. N.; Crosby, G. A. *J. Phys. Chem.* **1971**, *75*, 991.
(26) Chou, P.-T.; Wei, C.-Y.; Chang, C.-P.; Meng-Shin, K. *J. Phys. Chem.* **1995**, *99*, 11994.
(27) Cross, A. J.; Waldeck, D. H.; Fleming, G. R. *J. Chem. Phys.* **1983**, *78*, 6455.
(28) Klein, U. K. A.; Haar, H.-P. *Chem. Phys. Lett.* **1979**, *63*, 40.
(29) The observed deuterium effect on the proton-transfer time (1.6 ps/1.1 ps = 1.5) is smaller than is expected for reactions by quantum mechanical tunneling. It suggests that tunneling is not the major mechanism for the proton transfer of the 7-azaindole dimer in solution at room temperature.
(30) Konijnenberg, J.; Huizer, A. H.; Varma, C. A. G. O. *J. Chem. Soc., Faraday Trans. 2* **1988**, *84*, 1163.
(31) This radiative lifetime of the monomer is obtained by integration of the lowest-energy band of the monomeric absorption spectrum from 235 to 315 nm.
(32) In this literature, the quantum yield of the tautomeric fluorescence is written as 0.002. However, judging from their argument using the value, 0.002 is probably a misprint and the "real" value must be 0.02.
(33) Suzuki, T.; Okuyama, U.; Ichimura, T. *J. Phys. Chem. A* **1997**, *101*, 7047.
(34) Waluk, J.; Pakula, B.; Komorowski, S. J. *J. Photochem.* **1987**, *39*, 49.
(35) This radiative lifetime of 140 ns may be a shorter limit because the lowest-energy absorption band of 7-methyl-7*H*-pyrrolo[2,3-*b*]pyridine significantly overlaps with strong higher-energy absorption bands.
(36) Catalan, J.; Perez, P. *J. Theor. Biol.* **1979**, *81*, 213.
(37) Uncertainty in the evaluated oscillator strength values is estimated as around 30%. It comes predominantly from uncertainties in the quantum yield of the tautomer fluorescence and those in the fitting analysis of the fluorescence spectra using the Lorentzian functions.
(38) If the transition frequency at the absorption maximum (3.50×10^4 cm^{-1}) is used in this calculation instead of that at the fluorescence maximum ($\nu_{04} = 3.09 \times 10^4$ cm^{-1}), the radiative lifetime of $\tau_{r4} = 7.5$ ns is obtained. The fluorescence quantum yield of the monomeric excited state corresponding to this radiative lifetime is $\phi_4 = 1.02/7.5 = 0.136$.
(39) Badger, G. M.; Christie, B. J. *J. Chem. Soc.* **1956**, 3438.
(40) Ilich, P. *J. Mol. Struct.* **1995**, *354*, 37.
(41) Rich, R. L.; Chen, Y.; Neven, D.; Negrerie, M.; Gai, F.; Petrich, J. W. *J. Phys. Chem.* **1993**, *97*, 1781.
(42) Quantitative analysis of the fluorescence anisotropy change of the 7-azaindole dimer will be given elsewhere. Takeuchi, S.; Tahara, T. To be submitted.
(43) Nagaoka, S.; Nagashima, U. *J. Phys. Chem.* **1990**, *94*, 1425.
(44) Douhal, A.; Kim, S. K.; Zewail, A. H. *Nature* **1995**, *378*, 260.
(45) Douhal, A.; Guallar, V.; Moreno, M.; Lluch, J. M. *Chem. Phys. Lett.* **1996**, *256*, 370.
(46) Folmer, D. E.; Poth, L.; Wisniewski, E. S.; Castleman, A. W., Jr. *Chem. Phys. Lett.* **1998**, *287*, 1.
(47) Tokumura, K.; Watanabe, Y.; Itoh, M. *J. Phys. Chem.* **1986**, *90*, 2362.
(48) Chachisvilis, M.; Fiebig, T.; Douhal, A.; Zewail, A. *J. Phys. Chem. A* **1998**, *102*, 669.
(49) Iwata, K.; Hamaguchi, H. *J. Phys. Chem. A* **1997**, *101*, 632.
(50) Nilmoni, S.; Takeuchi, S.; Tahara, T. Manuscript in preparation.